RSC Advances

ROYAL SOCIETY OF CHEMISTRY

www.rsc.org/advances

RSC Advances

ARTICLE

A facile one-pot solvothermal synthesis of $CoFe_2O_4$/RGO and its excellent catalytic activity on thermal decomposition of ammonium perchlorate

Received 00th January 20xx,
Accepted 00th January 20xx

DOI: 10.1039/x0xx00000x

www.rsc.org/

Teng Chen[a], Ping Du[b*], Wei Jiang[a*], Jie Liu[a], Gazi Hao[a], Han Gao[a], Lei Xiao[a], Xiang Ke[a], Fengqi Zhao[c], Chunlei Xuan[c]

$CoFe_2O_4$/RGO hybrids have been successfully fabricated *via* a facile one-pot solvothermal method, which were characterized by X-ray diffraction (XRD), Raman, Fourier-transform infrared spectroscopy (FT-IR) and X-ray photoelectron spectroscopy (XPS). During this process, graphene oxide was reduced to graphene (RGO) and $CoFe_2O_4$ nanoparticles were deposited on the RGO. Scanning electron microscopy (SEM) and Transmission electron microscopy (TEM) revealed that the average size of $CoFe_2O_4$/RGO hybrids was 120nm, which was smaller than that of bare $CoFe_2O_4$, implying that RGO could effectively prevent $CoFe_2O_4$ nanoparticles from aggregating. To investigate the catalytic activity of the as-synthesized $CoFe_2O_4$ particles and $CoFe_2O_4$/RGO hybrids, the thermal decomposition of ammonium perchlorate (AP) was characterized by differential thermal analyser (DTA). Both of the two exothermic process were merged into a sole exothermic process with the addition of bare $CoFe_2O_4$ and $CoFe_2O_4$/RGO hybrids, though there was no change in the position of the phase transition temperature of AP. Moreover, the catalytic activity of $CoFe_2O_4$/RGO hybrids is higher than that of bare $CoFe_2O_4$, due to the large surface area and enhanced properties of RGO in the hybrids. The Temperature programmed reduction (TPR) measurements showed that the reduction temperature of $CoFe_2O_4$ /RGO decreased by 55 °C compared with bare $CoFe_2O_4$, which further confirmed the higher catalytic activity of $CoFe_2O_4$ /RGO of than that of $CoFe_2O_4$ nanocomposites. Hence, $CoFe_2O_4$/RGO hybrids could be a promising addictive in modifying the burning behaviour of AP-based composite propellant.

1. Introduction

In a typical formula, composite solid propellant consists of polymer (binder), energetic fuel and oxidizer salts.[1-4] Ammonium perchlorate (AP) is one of the main components in composite solid propellant, which has been extensively employed as an oxidizer for rocket propulsion. The High-temperature decomposition (HTD) properties of AP, such as the activation energy, rate and temperature can directly affect the combustion behaviour of composite solid propellant, including the burning rate and pressure exponent. With the development of modern rocket, even higher energy release rate is required. Thus it is important to decrease the pyrolysis temperature of AP, because the lower the HTD temperature, the higher the burning rate and the more exothermic heat will be.[5-8]

In order to decrease the pyrolysis temperature and improve the energy release rate of AP, transition metal particles and metal oxides have been extensively used to catalyse the reaction of AP.[9-13] It is known that the particle size of burning rate catalyst could affect the catalytic activity towards AP. Therefore, a nano-sized catalyst is more effective than a micron-sized catalyst, due to its smaller size, larger surface area and high-surface activity. However, nano-sized particles are inclined to agglomerate into large particles which lead to the decrease of their specific surface area and active sites.[14] Moreover, the formation of heterogeneous dispersion phase, caused by the agglomeration of nano-sized particles, can also inhibit the catalytic activity in the thermal decomposition process of AP. In order to prevent the nano-sized particles from agglomerating, the most commonly used method is to coat some chemical agents on the surface of nano-sized particles, such as polymers and ligands. The existence of these inert components, which are coated on the surface of nano-sized particles, may decrease their reaction activity and the total energy of composite solid propellant, thus severely limiting their practical application. Hence, it is necessary to explore an alternative method to prevent the aggregation and keep their high reaction activity. With this regards, various supporting materials have been widely studied, of which, graphene could be considered as an

[a] National Special Superfine Powder Engineering Research Center of China, School of Chemical Engineering, Nanjing University of Science and Technology, Nanjing 210094, China. Email:superfine_jw@126.com. Tel.: +86 2584315042. Fax: +86 25 84315042.
[b] School of Chemical Engineering, Nanjing University of Science and Technology, Nanjing 210094, China. Email: dp1314@163.com.
[c] Xi'an Modern Chemistry Research Institute, Xi'an 710065, China

ideal substrate for nano-particles to spread and distribute on, due to its large specific surface area and specific properties. [15-16]

Since graphene was discovered by Andre Geim's team,[17] it has attracted tremendous attention from scientific researchers[18-21]. It is well known that researchers have paid great attention to carbon nanotubes over the past few decades,[22-23] and nowadays, graphene takes a similar level in new applications as carbon nanotubes. Due to the two dimensional structure and extraordinary physical, chemical and mechanical properties of graphene[24], it was considered as a promising nanoscale building blocks for new materials, motivating the development of new materials in many fields,[25-29] such as batteries, sensors, catalyst, supercapacitors, and energy storage.

Up till now, numerous facile methods have been developed to prepare graphene sheets，such as mechanical cleavage, thermal expansion of graphite,[30-32] chemical vapour deposition[17,33] and chemical reduction of exfoliated graphite oxide to Reduced graphene oxide (RGO).[34-35] Among these methods, chemical reduction of exfoliated graphite oxides is the most convenient way. Several oxygen-containing functional groups, including hydroxyl, carboxyl and epoxy groups, are introduced into graphite oxides, which make it easily to reduce graphite oxides into RGO. The porous structure of RGO can not only improve the stability and dispersion of nano-sized particles, but can also enhance their properties.

At present, the catalytic behaviour of graphene-based metal oxides in the thermal decomposition of AP has been reported by previous studies.[28-32] Nevertheless, to the best of our knowledge, there was no other report of $CoFe_2O_4$/RGO hybrids.

In this work, $CoFe_2O_4$/RGO hybrids were prepared by a facile one-pot solvothermal method and their catalytic behaviour on the decomposition of AP was investigated by varying its content over the range of 1-5% by differential thermal analysis.

2. Experimental

2.1 Materials

Graphene oxide was purchased from Nanjing Jicang Nanotechnology Co., Ltd, Ferric chloride hexahydrate ($FeCl_3 \cdot 6H_2O$), Cobalt chloride hexahydrate ($CoCl_2 \cdot 6H_2O$), Sodium citrate ($Na_3C_6H_5O_7 \cdot 2H_2O$), Sodium acetate ($CH_3COONa$), Ethylene glycol ($HOC_2H_4OH$) were purchased from Sino pharm Chemical Reagent Co., Ltd. All of the chemicals were analytical grade, commercially available and used without further purification.

2.2 Synthesis of $CoFe_2O_4$/RGO hybrids

The $CoFe_2O_4$/RGO hybrids were prepared via a facile one-pot solvothermal in Ethylene glycol. In a typical procedure, 90 mg of GO was dispersed in 40 mL Ethylene glycol and ultra-sonicated for 2 h. Then 0.34 g of $CoCl_2 \cdot 6H_2O$ and 1.06 g of $FeCl_3 \cdot 6H_2O$ (the molar ratio of Fe:Co is 2:1) were added to the suspension of GO. The mixture was vigorously stirred with a magnetic stirrer for 30 min to form a stable and homogeneous solution. Subsequently, 0.2 g of Sodium citrate and 1.2 g of sodium acetate were slowly added to form a stable suspension. After mechanical stirring for 30 min, the resulting suspension was transferred to a 100 mL Teflon-lined stainless steel autoclave, tightly sealed and maintained at 180 °C for 12 h. After cooling down to room temperature, the obtained precipitate was centrifuged, washed thoroughly with deionized water and dried at 60 °C for 12 h. For comparison purpose, bare $CoFe_2O_4$ nanoparticles and RGO were also synthesized under the same experimental condition in the absence of GO or $CoCl_2 \cdot 6H_2O$ and $FeCl_3 \cdot 6H_2O$, respectively. The schematic diagram for solvothermal thermal synthesis of nanospheres is illustrated in Fig. 1.

2.3 Characterization

X-ray powder diffraction measurements of the samples were carried out using a Bruker D8-Advanced diffractometer with accelerating voltage 40 kV and current 40 mA of Cu Kα radiation (λ = 0.15406 nm), and the scanning angle of 2θ was in the range from 5° to 80°. Raman scattering spectra was performed to characterize the difference of the as-synthesized products with detecting section ranged from 500 to 4000 cm^{-1}. Fourier-transform infrared (FT-IR) spectra was recorded to detect the chemical bonds on a Bruker Vector 22 spectrometer at room temperature. Scanning electron microscope images (Model-S4800) were taken to investigate the morphology of the samples. The microscopic structure and size were further confirmed by transmission electron microscopy (TEM, Tecnai 12).

Information about the element composition was gained from X-ray photoelectron spectroscopy (XPS).The porous characteristics of the as-synthesized samples were measured by the nitrogen physical adsorption of at 77 K. Prior to the experiment, the sample was degassed under vacuum at 200 °C for 5 h. The specific surface areas of the resultant were estimated using the Brunauer–Emmett–Teller (BET) equation. The pore size distribution was obtained from the adsorption branch according to Barrett–Joyner–Halenda (BJH) method.

2.4 Catalytic measurement

The catalytic activity of RGO, $CoFe_2O_4$, and $CoFe_2O_4$/RGO hybrids on thermal decomposition of AP were investigated using differential thermal analyser (DTA) with a heating rate of 20 °C/min in a static nitrogen atmosphere over the temperature range of 50-500 °C. The mass ratio of RGO, $CoFe_2O_4$, and $CoFe_2O_4$/RGO hybrids in AP were 1%, 3%, 5%, respectively. The activation

energies of AP decomposition with and without $CoFe_2O_4$/RGO hybrids were measured under different heating rates. The Temperature programmed reduction (TPR) analysis was performed in the presence of 5% H_2/N_2 flow (50 mL/min) and the temperature was increased from ambient to 1000°C at 10 °C/min.

3 Results and discussion

The structure of the resulting samples was confirmed by XRD. Fig. 2 shows the XRD patterns of GO, $CoFe_2O_4$ and $CoFe_2O_4$/RGO. It can be seen that the original GO sample exhibits a sharp diffraction peak at 2θ=11.05°, corresponding to the (001) reflection. The observed diffraction peak at 30.1°, 35.4°, 43.1°, 53.5°, 56.9°, 62.6°can be indexed to the (220), (311), (400), (422), (511), (440) reflections, respectively. These peaks match well with the standard pattern of cubic spinel structure (JCPDS card 22-1086), indicating the formation of $CoFe_2O_4$.[36] It's noticeable that the characteristic diffraction peak at 11.05° disappears in the XRD pattern of $CoFe_2O_4$/RGO, which suggests that GO has been effectively reduced into graphene sheets. All characteristic diffraction peaks of $CoFe_2O_4$/RGO hybrids are accordance with bare $CoFe_2O_4$ particles. Meanwhile, no other diffraction peaks related with impurities are detected, which indicate $CoFe_2O_4$/RGO hybrids have been synthesized via a facile one-pot solvothermal method.

Fig. 1. Illustration of synthesis process of $CoFe_2O_4$/RGO

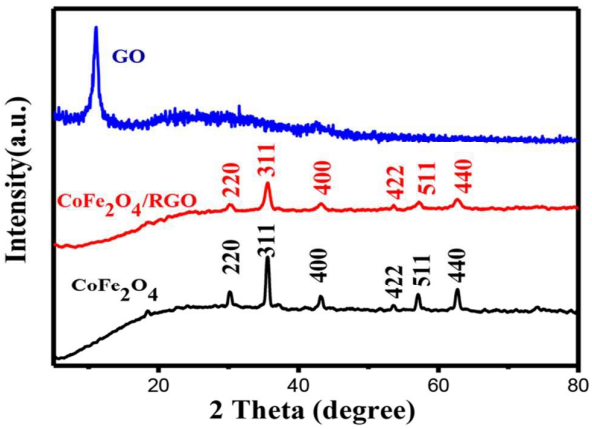

Fig. 2. XRD patterns of GO, $CoFe_2O_4$ and $CoFe_2O_4$/RGO hybrids

The functionalized groups on graphite oxide and $CoFe_2O_4$/RGO were then characterized by FT-IR spectrum. Fig. 3 (a) shows the FT-IR spectra of GO and the $CoFe_2O_4$ /RGO nanocomposites which were recorded between 4000 $cm^{-1}$and 500 cm^{-1}.The peak observed at 3620 cm^{-1} is attributed to the stretching vibration of -OH in the presence of adsorbed water. Several characteristic peaks related with the oxygen-containing functional groups can be found in Fig. 3 (a). The peaks at 1721, 1613, 1213 and 1041 cm^{-1} should be ascribed to the carboxy C=O, aromatic C=C, epoxy C-O and C-O groups on the surface of graphene sheets respectively. Compared with GO, Most characteristic peaks of the oxygen-containing functional groups on GO vanished in the spectrum of $CoFe_2O_4$/RGO, which implies that the oxygen-containing functional groups have already been removed from GO in the process of solvothermal.

In contrast to the peak at 1612 cm^{-1} in GO, a red shift peak around 1564 cm^{-1} can be observed in $CoFe_2O_4$/RGO, indicating the restoration of π-π conjugation of graphene sheets. The new absorption peak appeared at lower frequency around 554 cm^{-1} in $CoFe_2O_4$/RGO suggests that the Fe (Co)-O bonds have been formed in the presence of cobalt ferrite.[37] From the FT-IR spectrum, we can assume that graphite oxide has been reduced to RGO and the target product of $CoFe_2O_4$/RGO has been synthetized.

Raman spectroscopy is an efficient tool for detecting the structure of carbonaceous materials. The Raman spectra of GO, RGO and $CoFe_2O_4$/RGO hybrids are shown in Fig. 3 (b). It is obvious to observe that all of the spectra for GO, RGO and $CoFe_2O_4$/RGO display two peaks, which represent the G-and D-bands respectively. The G-band corresponds to the first-order scattering of the E_{2g} mode for SP^2-hybridized carbon and the D-band originates from intervalley scattering of disordered structure. Compared with those of GO, the peaks of D-bands shifted to lower frequencies. The D-band shifted from 1346 to 1336 cm^{-1}, indicating that GO has been reduced to RGO.[38] The intensity ratio (I_D/I_G) of D-band to G-band is correlative with the disorder and defects in graphene. It can be

observed that the I_D/I_G ratio of RGO (1.15) is higher than that of GO (1.01), suggesting the reduction of GO into RGO and more defects generated in RGO.[39-42] Metal or metal oxides nanoparticles can be easily trapped by the surface defects of RGO, which will result in the decrease of the defect density. It can be observed that I_D/I_G ratio of RGO in $CoFe_2O_4$/RGO is 1.11, which is lower than that of 1.15 in pristine RGO, implying that the defect density of RGO decreases after the decoration of $CoFe_2O_4$ nanoparticles on the surface of RGO.[43-45]

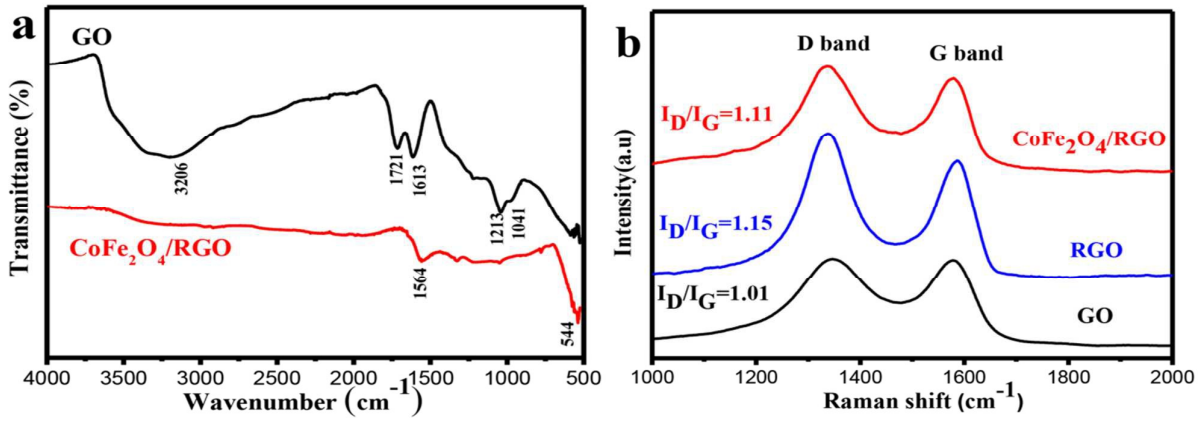

Fig. 3. FT-IR spectra of GO and $CoFe_2O_4$/RGO (a) and Raman spectra of GO, RGO and $CoFe_2O_4$/RGO (b)

The microstructure and morphology of the as-synthesized $CoFe_2O_4$/RGO hybrids were characterized by SEM and TEM. From the SEM images in Fig. 4, it can be clearly seen that graphene sheets are distributed between the $CoFe_2O_4$ nanoparticles, which can inhibit $CoFe_2O_4$ nanoparticles from aggregation. The TEM images of $CoFe_2O_4$/RGO are displayed in Fig. 5. It can be observed that $CoFe_2O_4$ nanoparticles are densely and uniformly decorated on the surface of crumpled graphene sheets. It should be pointed out that, no $CoFe_2O_4$ particles fell off graphene sheets after sonication for a long time in the process of preparing for TEM specimen. It indicates that the defect structures of RGO could trap $CoFe_2O_4$ nanoparticles[43, 44], which is accordance with result of the Raman analyses

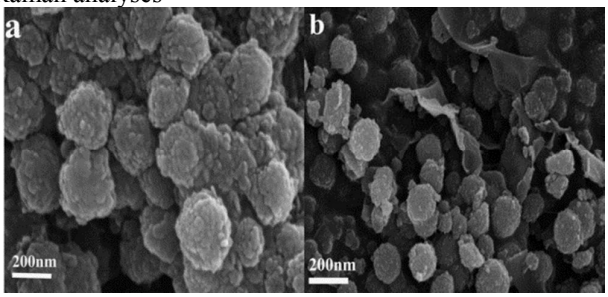

Fig. 4. SEM images of the as-synthesized $CoFe_2O_4$ (a); $CoFe_2O_4$/RGO hybrids (b).

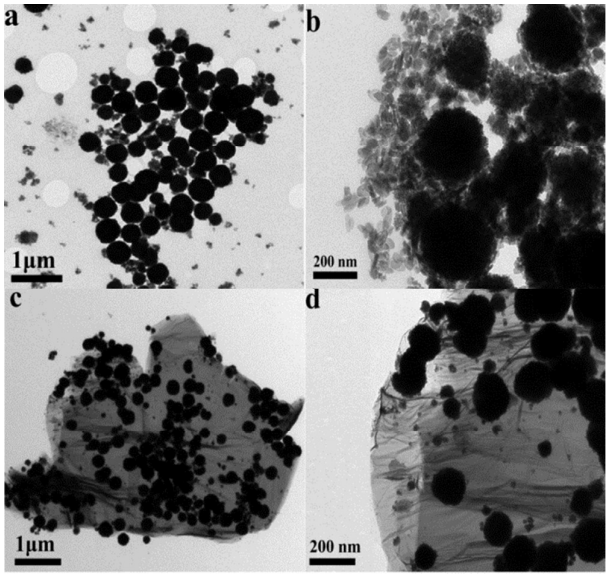

Fig. 5. TEM images of the as-synthesized $CoFe_2O_4$ (a, b); $CoFe_2O_4$/RGO hybrids (c, d).

Further evidence for chemical composition and valance state of elements in $CoFe_2O_4$/RGO hybrids were obtained by X-ray photoelectron spectroscopy (XPS). The wide scan XPS spectrum reveals the existence of Co (Co $2p_{1/2}$ and Co $2p_{3/2}$), Fe (Fe $2p_{1/2}$ and Fe $2p_{3/2}$), O (O1s) and C(C1s) element in $CoFe_2O_4$/RGO hybrids. The deconvolution of the Co 2p peak in $CoFe_2O_4$ and $CoFe_2O_4$/RGO are shown in Fig 6 (b). The peaks located at 780.5 eV and 796.3 eV in are assigned to Co $2p_{3/2}$ and Co $2p_{1/2}$, respectively. The accompanied shake up satellite

peaks at 786.6 eV and 803.5 eV confirm the oxidation state of Co^{2+} in the samples.[46] As illustrated in Fig 6 (c), the Fe $2p_{3/2}$ peak is cantered at 710.9eV and the Fe $2p_{1/2}$ peak is located at 724.8 eV. Two peaks appeared at 718.8 eV and 733.4 eV are ascribed to the shake up satellites of Fe $2p_{3/2}$ and Fe $2p_{1/2}$ respectively, indicating the existence of Fe^{3+}.[47] Compared with the Co 2p and Fe 2p spectra in $CoFe_2O_4$ and $CoFe_2O_4$/RGO, it can be inferred there is no shift in the binding energy of the peaks after decoration of $CoFe_2O_4$ on graphene sheets. The O 1s spectra in $CoFe_2O_4$ and $CoFe_2O_4$/RGO (Fig. 6 (d)) exhibit a large peak at 529.3 eV and 529.9 eV, respectively, corresponding to M-O-M, which is ascribed to the lattice oxygen in $CoFe_2O_4$ phase.[48] The other O 1s peak at 531.5 eV indicates the presence of oxygen containing groups which bonded with C atoms in RGO.[49] Fig. 6 (e) shows the C 1s spectra of GO, RGO and $CoFe_2O_4$/RGO. From the spectrum of GO, four de-convoluted peaks can be observed, which are related to C=C and C-C bonds (284.8 eV) in the aromatic rings, C-O bond (285.5 eV) of epoxy and alkoxy, C=O bond (287.7 eV) and O-C=O groups (288.8 eV), respectively.[50] In comparison with GO, the peak intensity of carbon-oxygen species in RGO decreases remarkably, indicating a effective reduction in the solvothermal process. Similar phenomenon can be observed in the spectrum of $CoFe_2O_4$/RGO. To further investigate the reduction degree of GO in $CoFe_2O_4$/RGO, the peak area ratios of oxygen-containing groups to total area are calculated according to the C1s spectrum and the results are depicted in Table 1. It can be concluded that the percentage of oxygen-containing groups has a remarkably decrease, which further confirms the reduction of GO in $CoFe_2O_4$/RGO hybrids.

Table. 1 Composition (Atom %) of the various carbon functional groups on the basis of the XPS results

Sample	C-C	C-O	C=O	COOH
GO	44.3	28.9	19.9	6.9
RGO	59.8	22.4	12.0	5.8
$CoFe_2O_4$/RGO	68.0	19.2	7.6	5.4

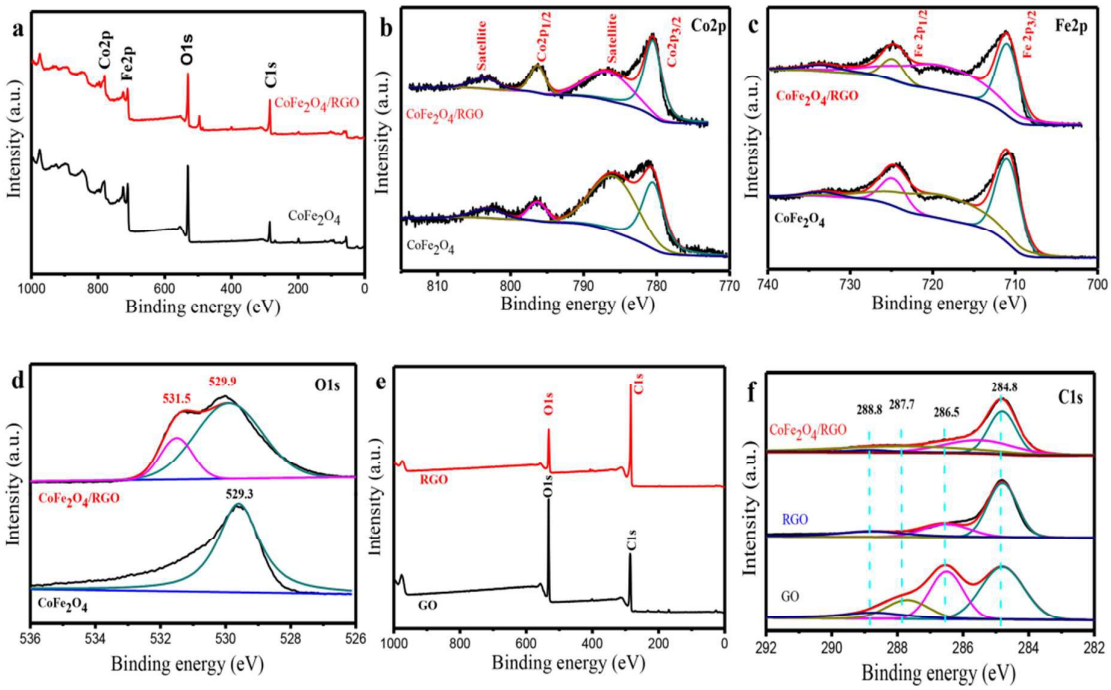

Fig.6. XPS survey spectra of the $CoFe_2O_4$/RGO and $CoFe_2O_4$ (a); XPS spectra for Co 2p of the $CoFe_2O_4$/RGO and $CoFe_2O_4$ (b); XPS spectra for Fe 2p of the $CoFe_2O_4$/RGO and $CoFe_2O_4$ (c); XPS spectra for O 1s of the $CoFe_2O_4$/RGO and $CoFe_2O_4$ (d); XPS survey spectra of the RGO and GO (e); XPS spectra for C 1s of the $CoFe_2O_4$/RGO, RGO and GO (f).

The specific surface area and the porosity distribution characteristic of the as-synthesized sample were investigated by N_2 adsorption-desorption at 77 K using N_2 as adsorbent. Fig. 7 shows the N_2 adsorption-desorption isotherms and porosity distribution curves. The isotherm demonstrates a typical "type Ⅳ" isotherm with H3 hysteresis loops, revealing the existence of mesoporous in $CoFe_2O_4$/RGO hybrids. The porosity distribution curve of $CoFe_2O_4$/RGO hybrids inserted in Fig. 7 (b) shows a narrow pore-size distribution at 3.04 nm and a broad pore-size distribution around 15.28 nm, indicating that the hybrids virtually comprise mesoporous structure and a minor fraction of microporous structure. The Brunauer-Emmett-Teller (BET) surface area is calculated to be 242.5

$m^2 \cdot g^{-1}$ and the average pore size is 7.25 nm. Nevertheless, the specific surface area and the average pore size of bare $CoFe_2O_4$ nanoparticles are 60.2 $m^2 \cdot g^{-1}$ and 18.79 nm, respectively. These results indicate that the surface area of $CoFe_2O_4$/RGO hybrids is relatively larger and the distribution of pore size is more uniform than those of bare $CoFe_2O_4$ nanoparticles.

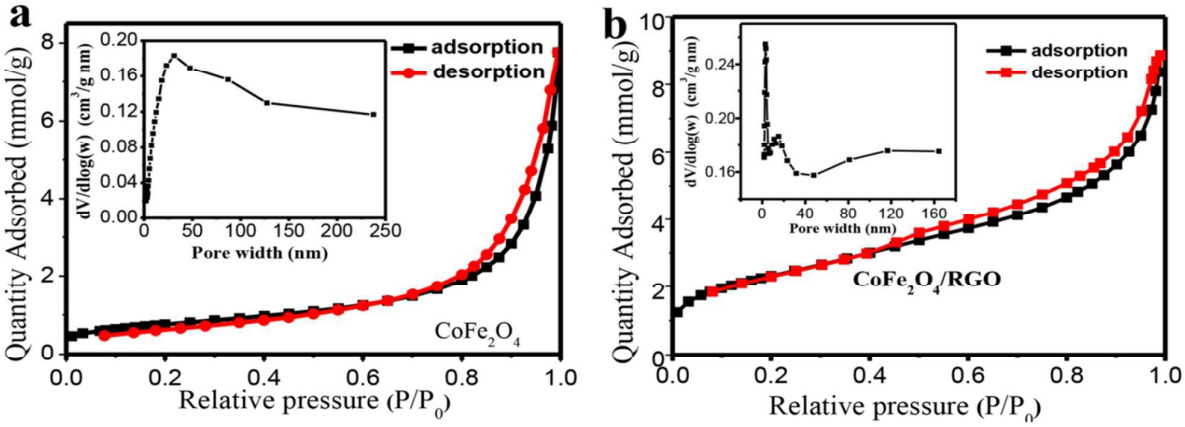

Fig. 7. Nitrogen adsorption-desorption isotherms of $CoFe_2O_4$ (a) and $CoFe_2O_4$/RGO hybrids (b).

The catalytic effect of the as-prepared $CoFe_2O_4$/RGO hybrids with different ratio in the thermal decomposition of AP was further investigated by DTA measurements at a heating rate of 20 °C/min. The DTA and TGA (thermogravimetric analysis) curves of pure AP and the as-prepared $CoFe_2O_4$/RGO hybrids are shown in Fig. 8. An endothermic peak centred at about 240 °C in all DTA curves corresponds to the crystallographic transition of AP from the orthorhombic to cubic form. Two obvious exothermic peaks appeared at about 320 °C and 440 °C for pure AP, represent the low-temperature decomposition (LTD) and high-temperature decomposition (HTD), respectively. Pure RGO has no catalytic behaviour on the decomposition of AP, as shown in Fig. 8 (a). When adding bare $CoFe_2O_4$ and $CoFe_2O_4$/RGO hybrids with different ratio to AP, two exothermic processes merge into a sole exothermic process, though there was no change in the position of the phase transition temperature of AP. For thermogravimetric analysis (TGA) of pure AP, two weight loss steps are observed as shown in Fig. 8 (d), which are attributed to the partial decomposition and complete decomposition of AP, respectively. While only one weight loss step is presented for AP mixed with $CoFe_2O_4$/RGO hybrids, which is consistent with DTA curves. Moreover, the catalytic activity is highly related with the amount of catalyst added, the decomposition temperature of AP gradually decreases with increasing the amount of catalyst. In the presence of bare $CoFe_2O_4$ (1%, 3%, 5%), the HTD temperature of AP is reduced by 77.6°C, 89.5°C, 95.2°C, respectively. Whereas, with the 1%, 3%, 5% addition of $CoFe_2O_4$/RGO hybrids, the HTD temperature of AP decreases by 92.3 °C, 104.7 °C, 113.6 °C, respectively. All the results manifest that both $CoFe_2O_4$ and $CoFe_2O_4$/RGO hybrids can promote the decomposition of AP. However, the catalytic activity of $CoFe_2O_4$/RGO hybrids is higher than that of bare $CoFe_2O_4$, due to the large surface area and enhanced properties of RGO in the hybrids discussed above, which is consistent with the theoretical expectation. Moreover, compared with the result reported in literature 51, the catalytic behaviour of $CoFe_2O_4$/RGO is higher than that of Fe_2O_3/graphene. The HTD temperature of AP mixed with 2% Fe_2O_3/graphene, is 367.0 °C, whereas, the HTD temperature of AP mixed with 1% $CoFe_2O_4$/RGO is 347.6 °C. This may be ascribed to the synergetic effect of Co^{2+} and Fe^{3+}.

To further investigate the catalytic behaviour of the as-sythesized $CoFe_2O_4$/RGO hybrids, DTA test with different heating rate were performed. Fig. 9 shows the DTA curves of pure AP and the mixtures of AP with $CoFe_2O_4$ and $CoFe_2O_4$/RGO at different heating rates.

The HTD kinetic parameters of AP with and without catalyst are calculated from the plot of exothermic peak temperature dependence as a function of heating rate.

The relationship between the decomposition temperature and heating rate can be dipicted by Kissinger correlation[52] and Arrhenius equation.

RSC Advances

ARTICLE

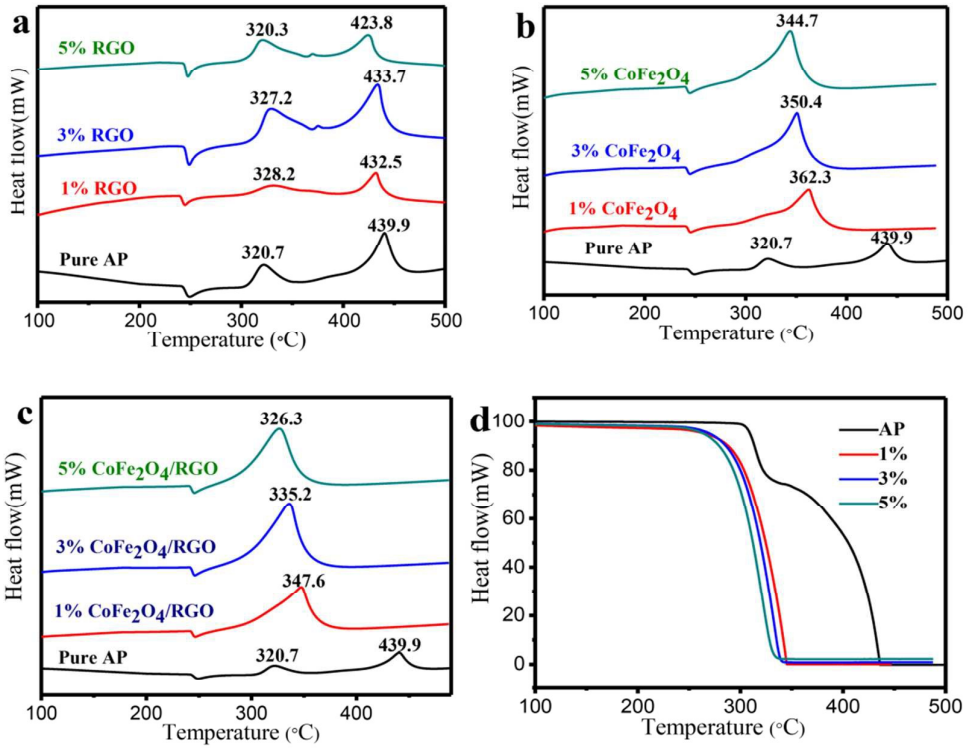

Fig. 8. DTA curves of Pure AP and AP mixed with RGO (1%, 3%, and 5%) (a), pure AP and AP mixed with $CoFe_2O_4$ (1%, 3%, and 5%) (b), Pure AP and AP mixed with $CoFe_2O_4$ /RGO hybrids (1%, 3%, and 5%) (c), TGA curves of pure AP and mixture of AP with $CoFe_2O_4$/RGO hybrids (1%, 3%, and 5%) (d).

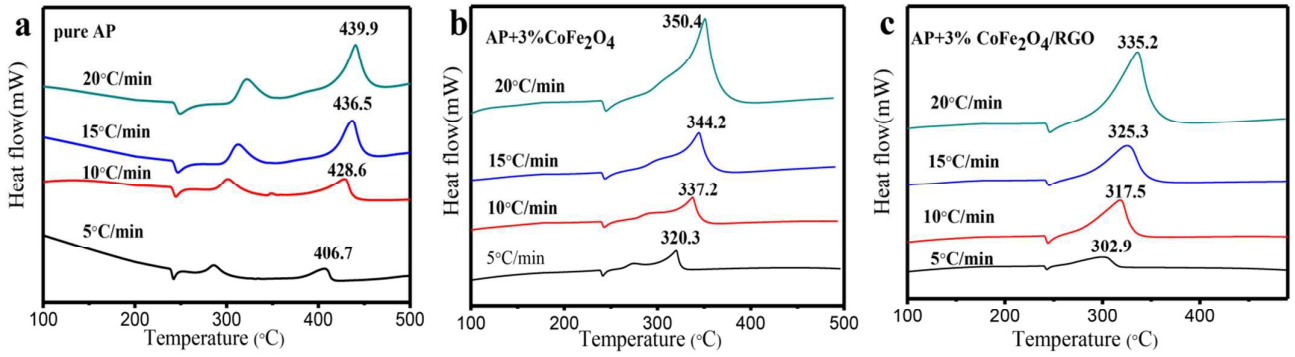

Fig. 9. DTA curves of pure AP (a) , AP mixed with 3% $CoFe_2O_4$ (b) and AP mixed with 3% $CoFe_2O_4$/RGO hybrids (c) at different heating rates.

RSC Advances

ARTICLE

$$\ln\left(\frac{\beta}{T_p^2}\right) = -\frac{Ea}{R\,T_p} + \ln\left(\frac{AR}{Ea}\right) \quad (1)$$

$$k = A \cdot \exp\left(-\frac{Ea}{R\,T_p}\right) \quad (2)$$

Where β is the heating rate in degrees Celsius per minute, Tp is the peak temperature, R is the ideal gas constant, Ea is the activation energy and A is the pre-exponential factor. k is the reaction rate constant. According to the equ (1), the term $\ln(\beta/T_P^2)$ varies linearly with $1/T_P$ yielding the kinetic parameters of activation energy from the slope of straight line. Fig.10 shows the experimentally measured $\ln(\beta/T_P^2)$ versus $1/T_P$ with and without catalyst. Table 2 shows the calculated kinetic parameters for pure AP, $CoFe_2O_4$/AP and $CoFe_2O_4$/RGO/AP in HTD processes. For pure AP, the activation energy of HTD is calculated to be 147.62 kJ/mol, which is similar to the reported value in the literature.[53] With the addition of $CoFe_2O_4$ nanoparticles and $CoFe_2O_4$/RGO hybrids, the activation energy of AP decomposition decreases to 131.47 kJ/mol and 117.91 kJ/mol, respectively. Besides, the k values for $CoFe_2O_4$ and $CoFe_2O_4$/RGO hybrids are up to about 30 and 50 times higher than pure AP. On the basis of the above data, both of the two kinds of additives show catalytic activity towards AP decomposition, and the catalytic activity of $CoFe_2O_4$/RGO is higher than that of bare $CoFe_2O_4$.

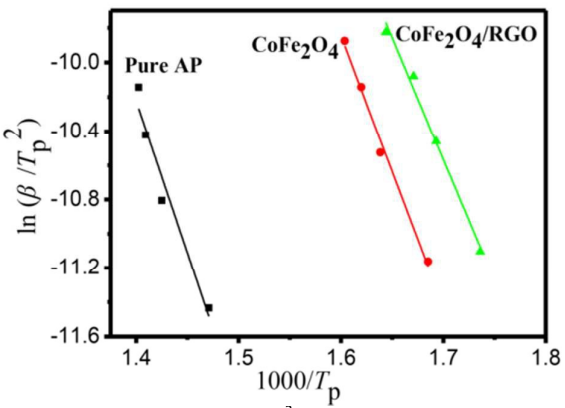

Fig. 10. Dependence of ln (β/Tp^2) on 1/Tp for AP and mixtures of AP with 3% additives. Scatter points are experimental data and lines denotes the linear fitting results.

Table 2. Summary of Kinetic parameters results for pure AP, $CoFe_2O_4$/AP and $CoFe_2O_4$/RGO /AP in HTD processes

Sample	Ea/kJ·mol^{-1}	A/min^{-1}	k/s^{-1}
Pure AP	147.62	4.02×10^{10}	2.35×10^{-3}
AP+ $CoFe_2O_4$	131.47	8.15×10^{10}	8.53×10^{-2}
AP+ $CoFe_2O_4$/RGO	117.91	1.08×10^{10}	1.27×10^{-1}

The particle size of catalyst and interaction between active centre and catalyst support can affect its reaction activity.[54] To probe the principle of high activity of $CoFe_2O_4$/RGO hybrids, H_2-TPR measurements were performed to investigate the reducibility of the catalysts. Fig. 11 showed the H_2-TPR profiles of $CoFe_2O_4$ nanoparticles and $CoFe_2O_4$/RGO hybrids. As shown in Fig. 11, two reduction peaks can be observed for $CoFe_2O_4$ and $CoFe_2O_4$/RGO: the first one can be ascribed to the reduction of CoO to metallic cobalt (Co^0) and Fe_2O_3 to Fe_3O_4, the second one might be interpreted as a reduction of Fe_3O_4 to FeO and Fe^0.[55] Compared with that of $CoFe_2O_4$ nanoparticles, the reduction temperature of $CoFe_2O_4$/RGO decreases by 26.2 °C. The downward shift in temperature implies that RGO can promote the reduction of $CoFe_2O_4$, hence, the $CoFe_2O_4$/RGO hybrids show the higher catalytic activity than $CoFe_2O_4$ nanocomposites.

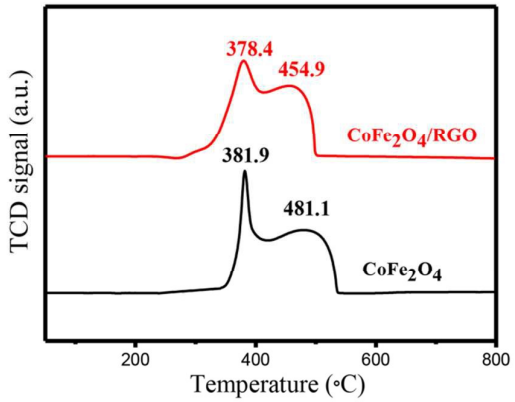

Fig. 11 H_2-TPR profiles of $CoFe_2O_4$ nanoparticles and $CoFe_2O_4$/RGO hybrids

Numerous researches were performed to reveal the mechanism of thermal decomposition of AP.[56-59] In this article, the mechanism of thermal decomposition of AP catalysed by $CoFe_2O_4$/RGO hybrids, has been explicated by adopting electron transfer mechanism.

The decomposition of AP undergoes three primary steps, the detail can be described as follows:

(1) The first step refers to the endothermic process, in which crystals of AP transform from the low-temperature orthorhombic phase to the high-temperature cubic phase.

(2) The second step represents the exothermic low-temperature decomposition (LTD) process of AP (300-330 °C), in which decomposition and sublimation take place. The scheme is shown as follows:

$NH_4ClO_4 \leftrightarrow NH_4^+ + ClO_4^- \leftrightarrow NH_3\ (g) + HClO_4\ (g) \leftrightarrow NH_3\ (s) + HClO_4\ (s)$

(3) In the third step, the exothermic high-temperature decomposition (HTD) process of AP (450-480 °C) would take place. In the HTD step, the heterogeneous decomposition of deprotonized $HClO_4$ would generate from the surface of reactant with the main products of N_2O, O_2, Cl_2, H_2O and a little NO.

In view of the above experimental findings, it can be inferred that $CoFe_2O_4$/RGO hybrids enhance both the LTD and HTD, due to the presence of RGO. A mechanism is proposed, as depicted in Fig. 12.

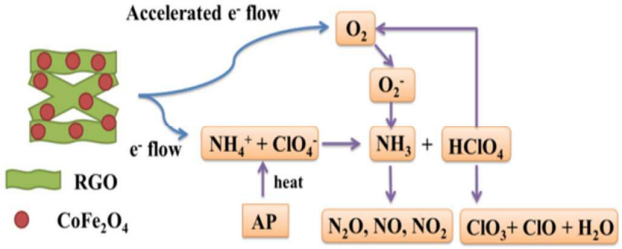

Fig. 12. Illustration of catalytic thermal decomposition process of AP by $CoFe_2O_4$/RGO hybrids.

Several hypotheses have been proposed to explain the decomposition mechanism of the AP catalysed by metal oxide additives, including the formation of easily melting eutectics between metal oxide additives and AP or intermediate amine compounds, and the release of O^{2-} ion.[59] In fact, the decomposition of AP involves two crucial steps: ammonia oxidation and dissociation of ClO_4^- species into ClO_3^- and O_2. In first step, metal oxides show high and stable catalytic activity and selectivity toward ammonia oxidation, thus promoting the AP decomposition. In second step, the ClO_4^- species in the presence of the oxide additives would decompose.[60]

For the low-temperature decomposition (LTD) process, in which the controlling step should be the electron transformation from ClO_4^- to NH_4^+, both gas and solid phase occur, involving dissociation and sublimation. While for HTD, it is associated with the transformation of O_2 to superoxide (O_2^-). According to the traditional electron-transfer theory, the presence of partially filled 3d orbit in Fe or Co atom provides help in an electro-transfer process. Positive hole in Fe or Co atom can accept electrons from AP ion and its intermediate products, by which the thermal decomposition of AP is accelerated. Due to the extraordinary conductivity of graphene, electrons can travel a lot faster and longer distance than they do among metal atoms without being scattered.[17,27] Thus, it can be concluded that the as-synthesized $CoFe_2O_4$/RGO hybrids with excellent electrical and conductive properties could provide more effective electrons and accelerate the two above mentioned thermal decomposition processes of AP. Namely, with the help of more effective and accelerated electrons, NH_4^+ and ClO_4^- can be easily transformed to NH_3 and ClO_4. Superoxide (O_2^-), which is transformed in a more efficient way from O_2 generated by $HClO_4$, could help NH_3 decompose into N_2O, O_2, Cl_2, H_2O and a little NO, completely.

In the absence of graphene, aggregated bare $CoFe_2O_4$ nanoparticles with low specific surface area and fewer active sites for adsorption gas phase molecules (NH_3, $HClO_4$) inhibit the decomposition of AP. However, when deposited on graphene sheet, which is a perfect catalyst carrier with a large surface area, the $CoFe_2O_4$ nanoparticles can fully unfold on the graphene sheet to form more effective active sites to react with NH_3 and $HClO_4$, and thus the catalysis effect is enhanced.

4. Conclusions

In conclusion, $CoFe_2O_4$/RGO hybrids have been successfully prepared by a facile one-pot solvothermal method. The average diameter of $CoFe_2O_4$/RGO hybrids is estimated to be 120 nm, which was confirmed by SEM and TEM, indicating that RGO could effectively prevent the $CoFe_2O_4$ nanoparticles from aggregating. The as-synthesized $CoFe_2O_4$/RGO hybrids exhibit highly catalytic activity on the thermal decomposition of AP, and the HTD temperature gradually decreases with the increase of catalyst. With 3% of $CoFe_2O_4$/RGO hybrids, the HTD temperature of AP is reduced by 104.7 °C, which is lower than that of bare $CoFe_2O_4$ under the same proportion. The results give the clear evidence that RGO can enhance the catalytic activity of $CoFe_2O_4$ and promote the thermal decomposition process, owing to its large surface area and enhanced properties of RGO. The facile preparation method depicted in this paper can be a promising and scalable technology for fabrication of other metal oxide/RGO hybrids with high catalytic activity for AP and AP based composite propellants. The improved catalytic activity, which is ascribed to the synergistic effect of nanoparticles and RGO may broaden a new application in modifying the burning behaviour of AP base composite propellant.

Acknowledgements

This work was financially supported by the National Natural Science Foundation of China (Project No. 41101287), the Scientific and Technical Supporting Programs of Jiangsu province (BE2012758), Priority

Academic Program Development of Jiangsu Higher Education Institutions and the Qin Lan Project.

Notes and references

[1] P. W. M. Jacobs and H. M. Whitehead, *Chem. Rev*., 1969, **69**, 551-590.
[2] A. G. Ajaz, J. *Hazard. Mater*., 1995, **42**, 303-306.
[3] I. P. S. Kapoor, P. Srivastava and G. Singh, *Propellants, Explos., Pyrotech*., 2009, **34**, 351-356.
[4] G. Singh, I. P. Singh, S. M. Mannan and J. Kaur J. *Hazard. Mater*., 2000, **79**, 1-18.
[5] V. Boldyrev, *Thermochim. Acta*, 2006, **443**, 1-36.
[6] S. Vyazovkin and C. A. Wight, *Chem. Mater*., 1999, **11**, 3386-3393.
[7] M. Shusser, F. E. C. Culick and N. S. Cohen, *J. Propul. Power*, 2002, **18**, 1093-1100.
[8] R. P. Fitzgerald and M. Q. Brewster, *Combust. Flame*, 2004, **136**, 313-326.
[9] A. Dey, V. Nangare, P. V. More, M. A. S. Khan, P. K. Khanna, A. K. Sikder and S. Chattopadhyay, *RSC Adv*., 2015, 5, 63777-63785.
[10] J. Zhao, Z. S. Liu, Y. L. Qin and W. B. Hu, *Cryst Eng Comm*, 2014, **16**, 2001-2008.
[11] D. Yan, H. Y. Zhao, Y. Liu, X. Wu and J.Y. Pei, *Cryst Eng Comm*, 2015, **17**, 9062-9069.
[12] Q. Li, Y. He and R.F. Peng, *New J. Chem*., 2015, **39**, 8703-8707.
[13] J. Cheng, R. X. Zhang, Z. L. Liu, L. X. Li, F. Q. Zhao and S.Y. Xu, *RSC Adv*., 2015,**5**,50278-50288.
[14]X. M. Chen, G.H. Wu, J.M. Chen, X. Chen, X. Chen, Z. X. Chen and X. R. Wang, *J. Am. Chem. Soc*.,2011,**133**, 3693-3695.
[15] Z.S. Wu, W. Ren, L. Wen, L. Gao, J. Zhao, Z. Chen, G. Zhou F. Li and H.M. Cheng, *ACS Nano*., 2010, **4**, 3187-3194.
[16] J.L. Yang, J.J. Wang, Y.J. Tang, D.N. Wang, X.F. Li, Y.H. Hu, R.Y. Li, G.X. Liang, T. K. Sham, and X.L. Sun, *Energy Environ. Sci*., 2013,**6** , 1521-1528.
[17] A.K. Geim, K.S. Novoselov, *Nat. Mater*., 2007, **6**,183-191.
[18] M.J. Allen, V.C. Tung, R.B. Kaner, *Chem. Rev*., 2009,**110**,132-145.
[19] S.Niyogi, E. Bekyarova, M. Itkis, J. McWilliams, M. Hamon, and R. Haddon, *J. Am. Chem. Soc*., 2006, **128**, 7720-7721.
[20] C.N.R. Rao, A. K. Sood, R.Voggu, K.S. Subrahmanyam, *J. phys. chem. Lett*., 2010,**1**,572-580.
[21] J.Wu, M. Agrawal, H. A. Becerril, Z. Bao, Z. liu, Y. Chen, P. Peumans, *ACS. Nano*, 2010, **4**, 43-48.
[22] B. Yue, Y. W. Ma, H. S. Tao, L. S. Yu, G. Q. Jian, X. Z. Wang, X. S. Wang, Y. N. Lu, and Z. Hu, *J. Mater. Chem*., 2008, **18**, 1747-1750.
[23] N. Mackiewicz, G. Surendran, H. Remita, B. Keita, G. Zhang, L. Nadjo, A.Hagege, E. Doris and C. Mioskowsk, *J. Am. Chem. Soc*., 2008, **130**, 8110-8111.
[24]H.J. Chen, M. Ishigami, C. Jiang, D.R. Hines, M. S. Fuhrer, E. D. Williams, *Adv. Mater*., 2007, **19**, 3623-3627.
[25] P. Blake, P.D. Brimicombe, R.R. Nair, T.J. Booth, D. Jiang, F. Schedin, L.A. Ponomarenko, S.V. Morozov, H. F. Gleeson,and E. W. Hill, *Nano Lett*., 2008, **8**, 1704-1708.
[26] A. Kezzima, N. Nasrallaha, A. Abdi and M. Trari, *Energy Convers. Manage*., 2011, **52**, 2800-2806.
[27] S. Stankovich, D. A. Dikin, G. H. B. Dommett, K. M. Kohlhaas, E. J. Zimney, E. A. Stach, R. D. Piner, S. T. Nguyen, and R.S. Ruoff, *Nature*, 2006, **442**, 282-286.
[28] L. P. Zhou, J. Xu, H. Miao, F. Wang and X. Q. Li, *Appl. Catal*., 2005, **292**, 223-236.
[29] L. Su, W. J. Qin, H. G. Zhang, Z. U. Rahman, C. L. Ren,S. D. Ma and X. G. Chen, *Biosens. Bioelectron*., 2015, **63**, 384-391.
[30] K. S. Kim, Y. Zhao, H. Jang, S. Y. Lee, J. M. Kim, K. S. Kim, J. H. Ahn, P. Kim, J. Y. Choi and B. H. Hong, *Nature*, 2009, **457**, 706-710.
[31] K. S. Novoselov, A. K. Geim, S. V. Morozov, D. Jiang, Y. Zhang, S. V. Dubonos, I. V. Grigorieva and A. A. Firsov, *Science*, 2004, **306**, 666-669.
[32] H. C. Schniepp, J. L. Li, M. J. McAllister, H. Sai, M. Herrera-Alonso, D. H. Adamson, R. K. Prud'homme, R. Car, D. A. Saville and I. A. Aksay, *J. Phys. Chem. B*, 2006, **110**, 8535-8539.
[33] A. Reina, X. T. Jia, J. Ho, D. Nezich, H. B. Son, V. Bulovic, M. S. Dresselhaus and J. Kong, *Nano Lett.*, 2009, **9**, 30-35.
[34] G. Eda, G. Fanchini and M. Chhowalla, *Nat. Nanotechnol.*, 2008, **3**, 270-274.
[35] X. B. Fan, W. C. Peng, Y. Li, X. Y. Li, S. L. Wang, G. L. Zhang and F. B. Zhang, *Adv. Mater.*, 2008, **20**, 4490-4493.
[36] I. C. Nlebedim, N. Ranvah, P. I. Williams, Y. Melikhov, J. E.Snyder, A. J.Moses and D. C.Jiles, *J. Magn. Mater*., 2010, **322**, 1929-1933.
[37]X. Fan, J.G. Guan, X.F. Cao, W. Wang, F.Z. Mou, *Eur. J. Inorg*.,Chem. 2010, **3**, 419-426.
[38] S. Stankovich, D. A. Dikin, R. D. Piner, K. A. Kohlhaas, A. Kleinhammes, Y. Jia, Y. Wu, S. T. Nguyen and R. S. Ruoff, *Carbon*., 2007, **45**, 1558-1565.
[39] W.D. Yang, Y. R. Li and Y.C. Lee, *Appl. Surf. Sci*., 2016, **380**, 249-256.
[40] D. L. Zhao, X. Gao, C. N. Wu, R. Xie, and S. J. Feng, *Appl. Surf. Sci*., 2016, **384**, 1-9.
[41] S. Q. Song, B. Cheng, N. S. Wu, A. Y. Meng, S. W. Cao and J. G. Yu, *Appl Catal. B: Environ*., 2016, **181**, 71-78.
[42] G. Q. Luo, X. J. Jiang, M. J. Li, Q. Shen, L. M. Zhang and H. G. Yu, *ACS Appl. Mater. Interfaces*., 2013, **5**, 2161−2168.
[43] J. A. Rodriguez-Manzo, O. Cretu and H. Banhart, *ACS Nano.,* 2010, **4**, 3422-3428.
[44] S. J. Jiang and S. Q. Song, *Appl Catal. B: Environ*., 2013, **140-141**, 1-8.
[45] C. C. Yeh and D. H. Chen, *Appl Catal. B: Environ*.,2014, **150-151**, 298-304.
[46] S. A. Chambers, R. F. C. Farrow, S. Maat, M. F. Toney, L. Folks, J. G. Catalano, T. P. Trainor and G. E. Brown, *Jr J. Magn. Magn. Mater*., 2002, **246**, 124-139.
[47] T. Yamashita and P. Hayes , *Appl. Surf. Sci.* 2008, **254**, 2441–2449.
[48] W. Y. Bian, Z. R. Yang, P. Strasser, and R. Z. Yang, *J. Power. Sources*., 2014, 250, 196-203.

[49] M. Zong, Y. Huang and N. Zhang, *Appl. Surf. Sci*., 2015, **345**, 272-278.
[50] H. Estrade-Szwarckopf, *Carbon*, 2004, **42**, 1713-1721.
[51] Y. Yuan, W. Jiang, Y, J. Wang, P. Shen, F. S. Li, P.Y. Li, F. Q. Zhao and H. X. Gao, *Appl. Surf. Sci*., 2014, **303**, 354-359.
[52] H.E. Kissinger, *Anal. Chem*., 1957, **29**,1702-1706.
[53]G. Tang, S.Q. Tian, Z.X. Zhou, Y.W. Wen, A.M. Pang, Y.G. Zhang, D.W. Zeng, H.T. Li, B. Shan, and C.S. Xie. *J. Phys. Chem. C*., 2014, **118**, 11833-11841.
[54] G. Fierro, M.L. Jacono and M. Inversi, *Appl. Catal. A: General*., 1996, **137** , 327–348.
[55] C. A. Chagas, E. F. de Souza, Marta C.N.A. de Carvalho, R. L. Martins and M. Schmal, *Appl. Catal. A: General*., 2016, **519** , 139-145.
[56]P. W. M. Jacobs and A. Russell-Jones, *J. Phys. Chem*., 1968,**72**, 202-207.
[57] S. S. Joshi, P. R. Patil and V. N. Krishnamurthy, *Def. Sci. J*.,2008, **586**, 721-726.
[58] L. Song, S. Zhang, B. Chen, J. Ge and X. Jia, *Colloids Surf*., A,2010, **360**, 1-5.
[59] V. V. Boldyrev, *Thermochim. Acta.*, 2006, **443**, 1-36.
[60] Y. F. Zhang and C. G. Meng. *J.Alloys Compd*., 2016, **674**, 259-265.

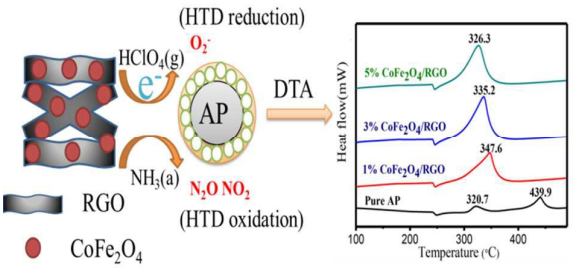

A novel catalyst of $CoFe_2O_4$/RGO has been synthesized and shows enhanced catalytic activity on thermal decomposition of ammonium perchlorate.